ELSEVIER

Journal of Chromatography A, 887 (2000) 199–208

JOURNAL OF CHROMATOGRAPHY A

www.elsevier.com/locate/chroma

Modelling of the pore flow in capillary electrochromatography

Remco Stol, Hans Poppe, Wim Th. Kok*

Polymer Analysis Group, Department of Chemical Engineering, University of Amsterdam, Nieuwe Achtergracht 166, 1018 WV Amsterdam, The Netherlands

Abstract

Pore flow in capillary electrochromatography (CEC) on porous silica particles has been investigated. To that end the migration behaviour of narrow polystyrene (PS) standards dissolved in di-methylformamide (DMF) with lithium chloride in 1 and 10 mmol/l concentration has been measured. These data have been compared to theoretical predictions. The latter were based on a model comprising cylindrical pores of varying diameter as measured experimentally by porosimetry, while the flow in each set of pores was calculated with the expression given by Rice and Whitehead. A reasonable to good agreement between experimental and predicted data was observed, provided it was assumed that pores of differing diameter occur in series. It was found that the flow in pores with a nominal size of 100 Å can be considerable compared to the interstitial flow, especially at 10 mmol/l ionic strength. It is concluded that pore flow within porous particles in CEC, of great importance for improved efficiency in both interactive and exclusion type CEC, can be predicted fairly reliably by means of the Rice and Whitehead expression.

Keywords: Pore flow; Modelling; Hydrodynamic radius; Electrochromatography; Polystyrene

1. Introduction

The concept of capillary electrochromatography (CEC) as a highly efficient alternative for high-pressure liquid chromatography (HPLC) has been introduced a considerable time ago [1,2]. Its implication in practice has been delayed because of various practical problems that had to be solved before the method could be used routinely. However, when Knox and Grant [3,4] had shown that it is possible to prepare highly efficient columns for CEC, and Smith and Evans [5] found a way to prevent the formation of gas bubbles in the columns, the interest in CEC grew considerably. Since then, an improvement of column performance, in comparison to pressure-driven systems, was shown by several other research groups (e.g., [6–10]).

In an electrically-driven system plate heights for a particular column are expected to be lower than in a pressure driven system, because of an improved mass transfer and a smaller influence of packing inhomogeneities. As the main advantage of CEC, however, it is generally seen that very small particles can be used as stationary phase material. In contrast to a pressure induced flow, the electroosmotic flow (EOF) in CEC is virtually independent of the particle size. A number of studies have been devoted to CEC with small (<3 μm) particles [4,5,11–14]. In some cases very low plate heights were obtained with these small particles, for instance as low as 2.0 μm [12] or even under 1.4 μm [15] with 1.5 μm non-porous particles. Still, in routine work CEC is

*Corresponding author.

0021-9673/00/$ – see front matter
PII: S0021-9673(99)01215-7

performed mostly with 3–5 μm particles, because columns with smaller particles are difficult to pack.

In our recent work [16] it was shown that the use of macroporous particles in CEC can be an alternative to that of very small particles. With 7 μm particles with nominal pore sizes of 500–4000 Å, plate heights were obtained down to 2.3 μm, i.e., to a reduced plate height of 0.34. The performance of these columns was similar to those packed with 1.8 μm material [14], while packing and operation proved to be considerably more simple. The high column efficiency with macroporous particles can be attributed to the existence of a considerable flow through the pores of the particles. As has been shown in perfusion chromatography [17,18], pore flow can drastically decrease the mass transfer contribution to the plate heights. Li and Remcho have also observed a decrease of plate heights attributed to pore flow in CEC with macroporous packing materials [19]. However, they observed these phenomena only with very wide pores and with high-ionic strength buffers. The existence of pore flow in chromatographic media under CEC conditions has been irrefutably proven by Venema et al. [20,21]. They showed that the retention window in size exclusion chromatography (SEC) could be much smaller with an electrically driven system than with a pressure driven system, the difference depending on the pore size and the ionic strength of the buffer used. Since the retention window in SEC reflects the difference in flow velocity of the mobile phase between and inside the particles, a considerable intraparticle flow must have been present in the electrically driven system.

For a proper description of the pore flow effects in CEC, and an intelligent optimisation of experimental parameters such as particle and pore sizes and buffer composition, a good model to describe the extent of flow in the pores of (modified) silica particles is required. Rathore and Horváth [22] have recently published a review on the different models that can be used for such a description. Since some of these models are quite complicated, most authors refer to the relatively simple model for EOF as presented by Rice and Whitehead [23]. Rice and Whitehead describe the effect of double-layer overlap on the EOF in narrow cylindrical channels and their model is used in CEC to describe the flow velocity and profile through a porous medium, such as the column. So far the validity of this model in CEC has not been tested. The model assumes a zeta potential independent of the channel diameter; this assumption is not trivial, because it relies on a complete charge regulation at the surface of the (modified) silica [24]. Moreover, in the derivation of the resulting equations the Debije Hückel approximation has been used, which is actually only valid for zeta potentials lower than those usually encountered on silica surfaces.

In the work presented here we have tried to validate the Rice and Whitehead model for the description of pore flow in CEC. For this, we have performed SEC experiments, using polystyrene standards as probe molecules of different sizes, with a column packed with a well defined silica material. The elution behaviour of the probe molecules was studied with pressure or an electric field as the driving force, using DMF with different salt concentrations as the mobile phase. The experimental results have been compared with predictions based on the Rice and Whitehead model. Attention is given to the effect of the pore size distribution on the resulting average pore flow velocity.

2. Experimental

2.1. Chemicals

N,*N*-Dimethylformamide (DMF), tetrahydrofuran (THF) and methanol were obtained from Acros (Geel, Belgium). Prior to use, the DMF was distilled under vacuum at 70°C to remove any possible ionic contaminants.

The polystyrene standards were purchased from Macherey Nagel (Düren, Germany) and had polydispersities between 1.03 and 1.30 as was specified by the supplier. Stock solutions of these polymers were prepared in either DMF or THF at a concentration of 10 mg/ml. Sample mixtures were prepared by mixing the stock solutions and dilution with the mobile phase to a concentration of 1.0 mg/ml. To all sample mixtures toluene was added, which served as the totally permeating marker.

The particles used as the column material (Lichrosorb 100–10) were obtained from Merck (Darmstadt, Germany). A relatively large particle diameter

was chosen to allow a comparison between pressure driven and electrically driven flow experiments.

The mobile phases consisted of either DMF or THF to which LiCl was added at concentrations of 1.0 and 10 m*M*. At a LiCl concentration of 0.1 m*M* significant secondary interactions took place between the stationary phase and the polystyrene, thereby restricting the successful mass calibration of the capillary SEC column. Therefore, these results were disregarded in the remainder of this work.

2.2. Apparatus

All experiments were performed on a HP^{3d}CE instrument (Hewlett Packard, Waldbronn, Germany). External pressure was delivered through a nitrogen gas bottle. Detection was performed by UV absorption at a wavelength of 260 nm. Although DMF has a UV cut-off at approximately the same wavelength, it was possible to detect the polystyrene, although relatively high concentrations had to be injected.

The same instrumental set-up was used for both the pressure and the electro drive experiments performed on the capillary columns. With the HP CE system, up to 12 bars of pressure can be applied on the column inlet, resulting in sufficiently high ($>$2.0 mm/s) linear velocities with columns made from 10 μm particles. This mode of operation is preferred over the use of a second instrumental set-up for the pressure drive experiments, since it allows direct comparison of the same column under both modes of operation and limits the risk of column damage.

The characterisation of the polystyrene standards was performed with a standard SEC system. The HPLC system consisted of a Spectroflow 757 solvent delivery system (ABI, Ramsey, NJ, USA) operated in the constant flow mode at 1.0 ml/min connected on-line to a Spectroflow 757 variable wavelength UV detector (ABI) operated at 254 nm and a viscosity detector model H502 (Viscotek, Oss, The Netherlands). The injection was performed with a Rheodyne type 7120 injector (Rheodyne, Berkeley, CA, USA) equipped with a 20 μl sample loop. The column was a 7.5 mm I.D. stainless steel column packed with 3 μm polymeric PLRP-S particles (cross-linked polystyrene-divinylbenzene) with 300 Å pores (Polymer Laboratories, Church Stretton, Shropshire, UK).

2.3. Particle characterisation

The pore-size distribution of the packing material was determined by mercury intrusion on a PASCAL 440 porosimeter (CE instruments, Austin, TX, USA). The skeleton density of the silica particles was measured with a 25 ml pycnometer (Micrometrics, Norcross, GA, USA).

2.4. Column preparation

At one end of a piece of fused-silica capillary (375 μm O.D. $\times$100 μm I.D., Polymicro Technologies, Phoenix, AZ, USA) a temporary frit was prepared by tapping it into a pile of dry silica particles (Hypersil 120-5 ODS, Hypersil, Astmoor, Runcorn, UK) and sintering them in place by heating locally with a small gas flame. A slurry containing 10 mg/ml of the packing material was prepared in methanol and homogenised by ultrasonification for 5 min. A 20 cm piece of stainless steel tubing with an I.D. of 1/16″ served as the slurry chamber and was filled with the slurry using a 3 ml syringe. The capillary was connected to the slurry chamber using standard LC connectors.

Next, high pressure was used to drive the particles into the capillary. The pressure was delivered by a high pressure membrane pump operated at an increasing pressure up to 500 bar. After 1 h at maximum pressure, the pressure was released slowly and the column was flushed with water for 30 min at a pressure of 150 bar. At this water pressure the permanent in- and outlet frits were prepared by heating locally with a hot metal strip device at a distance of 25 cm from each other. Then the pressure was released slowly and the column was reversely connected to the pump. At a pressure of 100 bars the remainder of the particles was flushed out of the capillary and a detection window was prepared immediately after the packed bed by burning of the protective polyimide coating using the hot metal strip device.

The column was then cut to the desired length and installed into the CE instrument. Next, the column was flushed with the mobile phase for 30 min by the application of 10 bars of headpressure at the column inlet. For the electro-driven experiments, the column was electrokinetically conditioned by the application

of a ramped voltage gradient of up to 25 kV across the column during 30 min.

3. Results and discussion

3.1. Characterisation of the stationary phase material

The density of the silica material was measured gravimetrically as 2.00 g/cm^3. Using a mercury porosimeter, the pore size distribution of the silica, with a nominal pore diameter of 100 Å, was determined. A clear distinction was found between the intra- and the interparticle void volume, with less than 4% of the total volume in the 50–500 nm pore size range. Therefore, a value of 50 nm was taken arbitrarily as the limit between the intraparticle pores and the interparticle space. The intraparticle pore volume was found to be 0.913 cm^3/g. In Fig. 1 the pore size distribution of the silica material studied is shown. For the intraparticle pores a fairly narrow distribution was found, with a volume-average pore diameter of 9.9 nm. The smallest pores measured had a diameter of 5 nm.

Since pore flow can be strongly dependent on the pore diameter, a further classification of the pores to size was made based on the measured distribution. The intraparticle pore volume was divided in 10%-fractiles; in Table 1 the diameter limits of the fractiles, and their median diameter, are given.

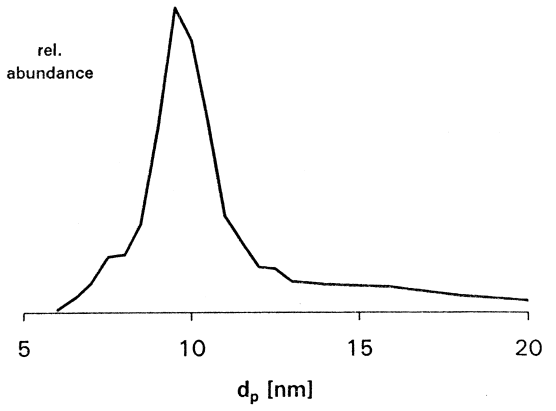

Fig. 1. The intraparticle pore size distribution of LiChrosorb Si 100.

Table 1
Size characteristics of the 10%-fractiles of the intraparticle pore volume of LiChrosorb Si 100

10%-volume fractile	Pore diameter limits (nm)	Median diameter (nm)
1	<8.2	7.5
2	8.2–8.9	8.7
3	8.9–9.3	9.1
4	9.3–9.6	9.4
5	9.6–9.9	9.7
6	9.9–11.0	10.4
7	11.0–14.0	12.1
8	14.0–18.8	16.0
9	18.8–28.0	22.7
10	28.0–50.0	35.2

3.2. Characterisation of the column

The total porosity of the column was determined. For this, the volumetric flow-rate was measured by weighing the change of the mass of the outlet vial during a series of pressure driven runs of in total 1.5–2 h length, taking into account the density of the solvent DMF (0.944 g cm^{-3} at 25°C). With every run the linear velocity of a marker analyte (toluene) was also measured. By comparing the volumetric flow velocity with the (average) linear flow velocity of the marker the total porosity of the column could be calculated. A total column porosity ε_{tot} of 0.80 ± 0.02 was found. Based on the data for the intraparticle pore volume and the density of the silica, the total column porosity can be divided into an intraparticle porosity ϵ_{in} of 0.37 and an interparticle porosity ε_{out} of 0.43. The latter value is higher than what is usually found for conventional HPLC columns; this may be attributed to a lower packing density (a relatively low pressure is used during packing) and to a more important wall effect.

3.3. Characterisation of the probe molecules

Since data on the size (hydrodynamic radius) of polystyrene molecules in DMF were not available in the literature, these were determined by SEC based on the principle of universal calibration [25]. The relation between the molecular mass and hydrodynamic radius of polystyrene in THF is well documented [26]. It can be described by the power law:

$$R_H(\text{THF}) = 0.0144 \times M_r^{0.561} \quad (1)$$

with the hydrodynamic radius R_H in nm and M_r = the molecular mass.

A standard SEC column was calibrated with PS standards using THF as the mobile phase. Toluene was used as the marker for the total mobile phase volume. The calibration curve of the relative migration volume τ as a function of log M_r was converted into a curve describing the relation between τ and log R_H for PS in THF, using the power law above. Next, τ values were measured for the PS standards with DMF as the mobile phase. R_H values in DMF were calculated by comparing the experimental τ values with the calibration line as measured with THF. In Fig. 2 the results are shown. It was found that the sizes of PS molecules in DMF are slightly larger than in THF, especially in the high M_r range. By regression of log R_H with log M_r the following power law was obtained for the hydrodynamic radius of PS in DMF:

$$R_H(\text{DMF}) = 0.0119 \times M_r^{0.588} \quad (2)$$

In further calculations the above expression was used to obtain R_H values for PS probe molecules of different sizes in DMF.

3.4. Column behaviour in pressure driven SEC

To predict the column behaviour under pressure-driven conditions, the intraparticle void volume was modelled as an ensemble of cylindrical channels with different diameters $d_{p,j}$, given by the means of the 10%-fractiles of the pore volume. Every spherical PS probe molecule i with a hydrodynamic radius $R_{H,i}$ will sample only a part ($f_{i,j}$) of the volume of a certain cylindrical channel j, with diameter $d_{p,j}$, due to the steric exclusion from the wall of the channel. The fraction f_i of the total intraparticle volume sampled by a certain PS molecule can be estimated as:

$$f_i = \sum_{j=1}^{10} f_{i,j} = \sum_{j=1}^{10} \frac{(d_{p,j} - 2R_{H,i})^2}{d_{p,j}^2} \; (\text{for } d_p > 2R_{H,i}) \quad (3)$$

In Table 2 the hydrodynamic radii of the PS standards used are given and the calculated fraction of the pore volume sampled by these probe molecules.

In pressure driven SEC the linear velocity of a probe molecule (u_i) is determined by its distribution between the flowing mobile phase between the particles and the stagnant mobile phase in the pores of the particles that is sampled:

$$u_i = u_{out} \cdot \frac{\varepsilon_{out}}{\varepsilon_{out} + \varepsilon_{in} \cdot f_i} \quad (4)$$

The excluded volume for the marker (toluene) is not completely negligible. With a radius estimated as 0.25 nm (calculated from its molar volume) the sampled fraction of the intraparticle space for toluene (f_0) is calculated to be 0.91.

The retention factor τ_i of a probe molecule, its retention volume divided by that of the low-M_r marker, can then be estimated as:

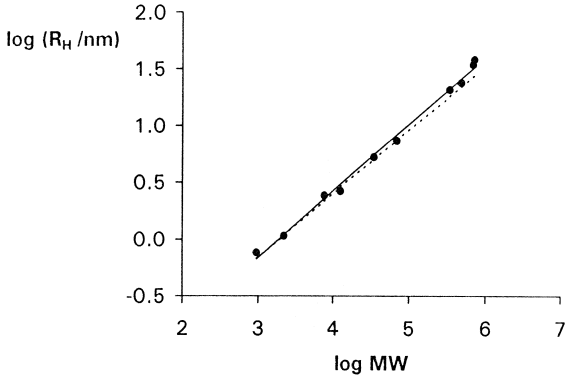

Fig. 2. Relation between the hydrodynamic radius and molecular mass for PS standards in DMF. (●): experimental values; (———): regression line; (- - -): regression equation in THF.

Table 2
Hydrodynamic radii and sampled fractions of the intraparticle pore volume of the PS standards used

M_r (kD)	R_H (nm)	f_i
0.95	0.7	0.78
2.2	1.1	0.66
7.6	2.3	0.38
12.5	3.1	0.25
19.8	4.0	0.15
43.9	6.4	0.06
97.2	10.2	0.02
336	21.1	0.00

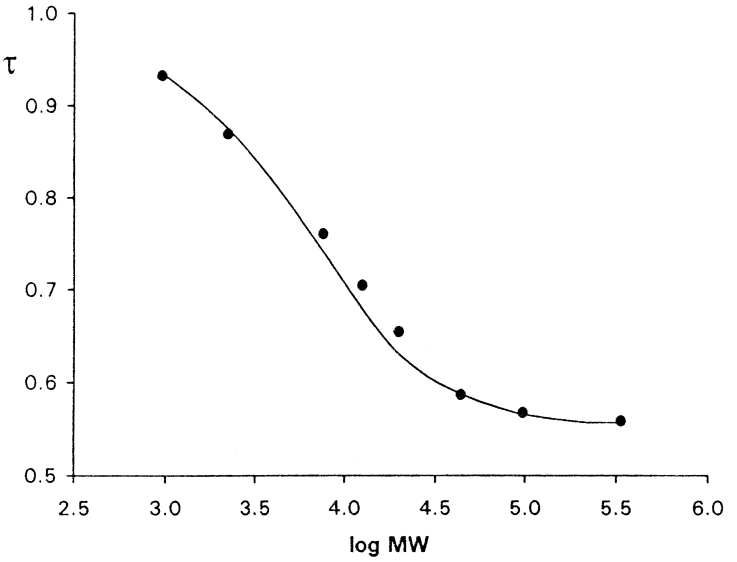

Fig. 3. Relative retention of PS standards in a pressure driven system. (●): experimental values; (———): prediction. DMF with 1.0 m*M* LiCl.

$$\tau_i = \frac{\varepsilon_{out} + \varepsilon_{in} \cdot f_i}{\varepsilon_{out} + \varepsilon_{in} \cdot f_0} \quad (5)$$

In Fig. 3 the experimental τ-values for polystyrene standards, measured under pressure-driven conditions, are compared with the predictions based on the porosity measurements. As is clear from the figure, there is a satisfactory agreement between the model and the experimental results.

3.5. Pore flow models

In wide channels, with a width well exceeding the thickness of the electric double-layer on the wall, the electroosmotic mobility is independent of the channel width. However, when the dimensions of the channel approach that of the double layer, the EOF is suppressed by the so-called double layer overlap. Rice and Whitehead [23] have derived an expression describing the effect of double-layer overlap on the electroosmotic velocity in thin cylindrical channels:

$$\omega = 1 - \frac{2I_1(d_p/2\delta)}{(d_p/2\delta) \cdot I_0(d_p/2\delta)} \quad (6)$$

where ω is the electroosmotic velocity relative to that in a wide channel, d_p is the channel diameter, δ the electrical double-layer thickness and I_0 and I_1 are zero-order and first-order modified Bessel functions of the first kind, respectively.

Electroosmotic velocities measured in packed columns can not be compared directly to EOF values measured in wide, open capillaries. First, corrections have to be made for the difference in field strength in the packed and open parts of a CEC column [27]. Moreover, due to the tortuosity of the streamlines in a packed bed, giving both a longer migration distance and a lower effective field strength, the apparent electroosmotic mobility in a packed bed will always be lower than in an open capillary under comparable experimental conditions. However, in first instance it can be assumed that the tortuosity for streamlines between particles in a packed bed is the same as the tortuosity through the pores of the particles. When such an assumption is justified, the ω-value as given in Eq. (6) predicts the velocity of the flow in a pore of a particle in comparison to the mobile phase velocity in the interparticle space.

To describe the effect of the pore size distribution on the average pore flow velocity two different

models have been used. In the first model the pores are regarded as an ensemble of parallel cylindrical channels with different diameters. This model would be adequate when a probe molecule would be transported through a certain channel or pore with a relatively uniform width over a relatively long distance before entering a next pore with a different diameter. The pore flow velocity is a strong function of the pore diameter. Fig. 4 shows the relative flow velocities, calculated with Eq. (6), for the different channel diameters representing the 10%-fractiles of the pore volume, for two different values for the ionic strength of the DMF solution. The flow in the wider channels has a strong influence on the average pore flow velocity. The volume-average pore flow velocity ($\overline{\omega}_{vol}$) in this parallel channel model is given by:

$$\overline{\omega}_{\mathrm{vol}} = \frac{\sum_{j=1}^{10} \omega_j}{10} \tag{7}$$

The second model describes the pores in the stationary phase material as an ensemble of cylindrical channels with different diameters in series. This model would be adequate when the probe molecules would follow pathways through pores or channels with a continuously changing width, or channels continuously splitting up and merging. The varying degree of double-layer overlap in such a non-uniform channel would be levelled out by parabolic flows. The resulting average flow velocity $\overline{\omega}_{fr}$ is the weighted average of the velocity in the different parts of the channel, with the flow resistance ($1/d_{p,j}^2$) as the weight factor:

$$\overline{\omega}_{fr} = \frac{\sum_{j=1}^{10} (\omega_j / d_{p,j}^2)}{\sum_{j=1}^{10} (1/d_{p,j}^2)} \tag{8}$$

In this series model the average pore flow velocity is dominated by the flow-rate in the narrow channels. In Table 3 the pore flows predicted with the two models are compared.

Both models have been used to predict the velocities of PS standards of different M_r in an electrically driven SEC system. In the parallel model, each 10%-fractile of the pore volume has its own relative flow velocity; the average velocity of a probe molecule depends on the volume fraction sampled of these 10%-fractiles:

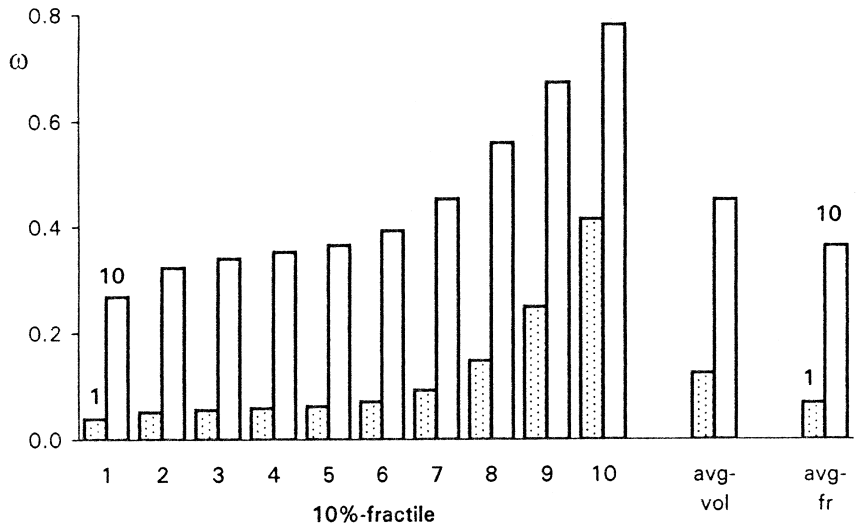

Fig. 4. Calculated relative pore flow velocities in channels representing the 10%-fractiles of the pore volume. DMF with 1 and 10 m*M* LiCl. For comparison the volume-averaged and the flow-restriction averaged values are also shown.

Table 3
Predictions of the average pore flow velocity and exclusion limits (τ_{excl}) by the parallel and series channel models

LiCl concentration (m*M*)	1	10
δ (nm)	6.51	2.06
Parallel model, $\overline{\omega}_{vol}$	0.124	0.450
Series model, $\overline{\omega}_{fr}$	0.068	0.363
Parallel model, τ_{excl}	0.59	0.75
Series model, τ_{excl}	0.57	0.70
Pressure driven, τ_{excl}	0.54	0.54

$$u_i = u_{out} \cdot \frac{\varepsilon_{out} + \varepsilon_{in} \cdot \sum_{j=1}^{10} f_{i,j} \cdot \omega_j}{\varepsilon_{out} + \varepsilon_{in} \cdot f_i} \quad (9)$$

Compared to the pressure-driven mode, the model predicts an increase of all probe molecule velocities compared to that of a totally excluded compound, i.e., a general loss of mass selectivity. Also, it predicts that the loss of selectivity is strongest in the high M_r range. These high M_r compounds sample only the widest pores, with the highest pore flow velocities, so that the velocities of these compounds come even more close to that of a totally excluded compound.

The series model implies that the flow velocities in wider and narrower parts of the pores are levelled out to a flow-resistance averaged value. The linear velocity of a probe molecule is now only determined by the fraction of the total pore volume it samples:

$$u_i = u_{out} \cdot \frac{\varepsilon_{out} + \varepsilon_{in} \cdot f_i \cdot \overline{\omega}_{fr}}{\varepsilon_{out} + \varepsilon_{in} \cdot f_i} \quad (10)$$

Again, a general loss of selectivity is predicted, albeit to a smaller extent than in the previous model because the average pore flow velocity is lower. The loss of selectivity is not especially strong for large molecules, because the flow velocity in the widest parts of the pores is assumed to be levelled out to the average value.

3.6. Column behaviour in electrically driven SEC

Mixtures of PS standards have been separated in the ED-SEC mode with an applied voltage of 15 kV. As the mobile phase DMF solutions of 1 m*M* and 10 m*M* LiCl were used. Experiments on the conductivity of DMF solutions of LiCl showed that ion association does not play a role in this concentration range. Therefore, the concentrations could be taken as the ionic strength of the solutions.

As had been observed previously [20,21], the retention window, the difference in retention time between a totally excluded compound and the low-M_r marker, was smaller than in the pressure driven mode, the decrease being most manifest with a high mobile phase ionic strength. In Fig. 5 the experimental τ-values for the PS standards are compared with the predictions based on the two models that have been elaborated. The predictions of the series channel model are closest to the experimental results. The pore flow velocity predicted by the parallel channel model is apparently too high. Moreover, the extra loss of selectivity in the high-M_r range predicted by this model is not found in practice.

4. Conclusions

It is of great importance to be able to predict the pore flow velocity in CEC, because it improves efficiency, especially when not-too-small particles are used. SEC experiments allowed a direct assessment of the extent of pore flow. The results of such experiments indicate that the Rice and Whitehead theory gives a good prediction of the relative pore flow velocity in packed CEC columns. However, the theoretical calculations show that not only the average pore diameter of the stationary phase is important, but also its pore size distribution. Different stationary phase materials with the same average pore size but different distributions could give strongly different perfusion rates. Moreover, the microstructure of the particles is to be taken into account. For the particular stationary phase material studied, the agreement between experimental results and theoretical predictions is best for the series model, which describes the pores as an ensemble of channels with a continuously changing diameter. With this model a flow-resistance averaged pore flow

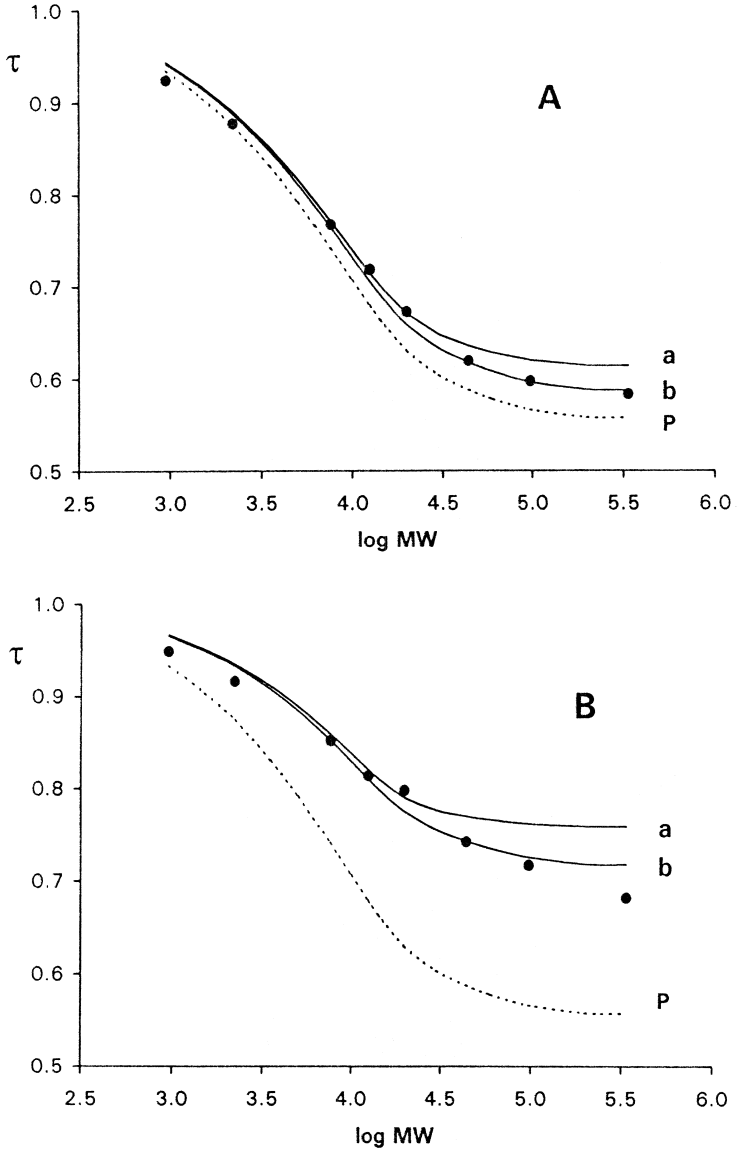

Fig. 5. Relative retention of PS standards in an electrically driven system. (●): experimental values; (———): predictions with the parallel (a) and series (b) models; (- - -): prediction for a pressure driven system. (A): 1 m*M* LiCl; (B): 10 m*M* LiCl.

velocity can be calculated using the Rice and Whitehead equation. However, it is well possible that with other types of particles or for instance mixed beds another model is more adequate to predict the pore flow.

Acknowledgements

This work was financially supported by the Netherlands Organization for Scientific Research (NWO) (grant no. 79.030). Thanks are due to Ms.

M.C. Mittelmeyer-Hazeleger for carrying out the porosity measurements.

References

[1] V. Pretorius, B.J. Hopkins, J.D. Schieke, J. Chromatogr. 99 (1974) 23.
[2] J.W. Jorgenson, K.D. Lukacs, J. Chromatogr. 218 (1981) 209.
[3] J.H. Knox, I.H. Grant, Chromatographia 24 (1987) 135.
[4] J.H. Knox, I.H. Grant, Chromatographia 32 (1991) 317.
[5] N.W. Smith, M.B. Evans, Chromatographia 38 (1994) 649.
[6] H. Rebscher, U. Pyell, Chromatographia 38 (1994) 737.
[7] M.M. Dittman, K. Wienand, F. Bek, G.P. Rozing, LC·GC 13 (1995) 800.
[8] C. Yan, R. Dadoo, H. Zhao, R.N. Zare, D.J. Rakeshaw, Anal. Chem. 67 (1995) 2026.
[9] S.E. van den Bosch, S. Heemstra, J.C. Kraak, H. Poppe, J. Chromatogr. A 755 (1996) 165.
[10] R.M. Seifar, S. Heemstra, W.Th. Kok, J.C. Kraak, H. Poppe, J. Microcolumn Sep. 10 (1998) 41.
[11] H. Yamamoto, J. Baumann, F. Erni, J. Chromatogr. 593 (1992) 313.
[12] R.M. Seifar, W.Th. Kok, J.C. Kraak, H. Poppe, Chromatographia 46 (1997) 131.
[13] S. Ludtke, T. Adams, K.K. Unger, J. Chromatogr. A 786 (1997) 229.
[14] R.M. Seifar, J.C. Kraak, W.Th. Kok, H. Poppe, J. Chromatogr. A 808 (1998) 71.
[15] R. Dadoo, R.N. Zare, C. Yan, D.S. Anex, Anal. Chem. 70 (1998) 4787.
[16] R. Stol, W.Th. Kok, H. Poppe, J. Chromatogr. A 853 (1999) 45.
[17] A.E. Rodrigues, J.C. Lopes, Z.P. Lu, J.M. Loureiro, M.M. Dias, J. Chromatogr. 590 (1992) 93.
[18] K.H. Hamaker, R.M. Ladisch, Sep. Purif. Meth. 25 (1996) 47.
[19] D. Li, V.T. Remcho, J. Microcolumn Sep. 9 (1997) 389.
[20] E. Venema, J.C. Kraak, R. Tijssen, H. Poppe, Chromatographia 58 (1998) 347.
[21] E. Venema, J.C. Kraak, H. Poppe, R. Tijssen, J. Chromatogr. A 837 (1999) 3.
[22] A.S. Rathore, Cs. Horváth, J. Chromatogr. A 781 (1997) 185.
[23] C.L. Rice, R. Whitehead, J. Phys. Chem. 69 (1965) 4017.
[24] B.V. Zhmud, J. Sonnefeld, J. Chem. Soc. Faraday Trans. 91 (1995) 2965.
[25] H. Benoit, Z. Grubisic, P. Rempp, D. Dekker, J.G. Zilliox, J. Chim. Phys. 63 (1966) 1507.
[26] L.J. Fetters, N. Hadjichristidis, J.S. Lindner, J.W. Mays, J. Phys. Chem. Ref. Data 23 (1994) 619.
[27] A.S. Rathore, Cs. Horváth, Anal. Chem. 70 (1998) 3069.